Article

A Highly Accurate Mathematical Model for Analyzing Modular Multilevel Converters in Transformer-Less Applications

Jinshuo Liu [1], Wenhua Xu [2],* and Tao Xu [1]

1   School of Control Science and Engineering, Shandong University, Jinan 250061, China
2   Network Information Technology Department, Shandong University, Jinan 250199, China
*   Correspondence: xuwenhua@sdu.edu.cn

Abstract: Transformer-less connection schemes can provide a feasible solution for lowering the economic cost, occupied space, and device weight of modular multilevel converter (MMC) systems. However, due to the reduction in the converter transformer, the current flow loop is changed; as a result, the existing MMC model is not suitable. In this paper, the ac- and dc-side equivalent circuit models of the MMC system using a transformer-less connection scheme are established in both a–b–c stationary and d–q rotating coordinate systems. Then, a highly accurate mathematical analysis model is proposed, in which the interactions among the electrical quantities can be fully seen. The mathematical model is established in the time domain, and hence the amplitude and phase angle of every harmonic component in each quantity can be directly obtained. The proposed model is verified under various typical situations by comparing the calculated values with the actual waveforms. The comparison results prove that the calculation error is small enough to be negligible. The mathematical model in this paper can provide a powerful tool in terms of the performance analysis and the main circuit parameter design for MMCs in transformer-less applications.

Keywords: modular multilevel converter; transformer-less application; mathematical model; performance analysis

1. Introduction

Voltage source converters (VSC) have gained more and more attention in both academia and industry [1]. In the past ten years, several kinds of VSCs have been developed and commercialized in the form of standard and customized products; among them, the modular multilevel converter (MMC) is a highly regarded topology [2,3]. In comparison with conventional two- and three-level converter topologies, the MMC has the following prominent advantages: (1) less harmonic distortion and fewer switching losses; (2) no direct serial connections of the semiconductor devices; and (3) modularity and scalability to meet any voltage level requirement [4–6]. Due to these advantages, the MMC has become the most widely used topology in VSC-based high-voltage direct current (VSC-HVDC) systems [7]. Moreover, it is considered a promising technology for renewable energy integration [8–10], medium-voltage reactive power compensation [11,12], electric transportation [13–15], and so on.

In the MMC-based conversion system, the converter transformer can contribute significantly to the converter station space, weight, and cost. Due to the excellent ac-side output performance of MMCs, a transformer-less operation can provide a more economical solution for MMC-based systems. In [16], a transformer-less MMC-based static synchronous compensator was proposed, and the operation control strategy and capacitor voltage balancing method were presented in detail. In the paper, the feasibility and effectiveness of a transformer-less operation were demonstrated. Then, an improved transformer-less MMC-based static synchronous compensator was proposed in [17] to achieve a better compensatory performance for high-power applications. The authors of another paper [18]

carried out a study on the control of a transformer-less MMC-HVDC system during asymmetric ac grid faults, which demonstrated the fault ride-through capability of the MMC in transformer-less applications. In [19], a third-order harmonic voltage suppression method was proposed for the five-level modular composited converter in transformer-less applications; based on the method, the ac-side zero-sequence current of the MMC could be effectively suppressed. Third-order harmonic voltage was further studied in [20], and a conclusion was drawn that the transformer-less connection could make the MMC have the potential to induce ac-side zero-sequence currents. In the paper, a proportional-resonant-based (PR-based) control strategy was proposed to suppress the unwanted harmonic current. The authors of another paper [21] carried out a study to demonstrate the feasibility of using a transformer-less MMC in a hybrid ac/dc power distribution system. The interaction influences of the ac and dc systems were analyzed. The paper also concluded that a transformer-less scheme can save economic costs and space, which are critical issues in power distribution systems.

The transformer-less connection scheme's feasibility and application potential have been demonstrated by existing studies [16–21], and the consensus is that it can make MMC-based ac/dc systems more economic and lightweight especially in medium- and high-voltage situations. However, at present, the research on MMCs in transformer-less applications is still shallow, and many issues require further study. One of the most urgent problems is that there is a lack of highly accurate mathematical models. The interactions among the electrical quantities in MMCs were studied in [22,23]; the fundamental mathematical models that can describe these interactions were established. Taking into account the influence of circulating current injections, an improved mathematical model was proposed in [24]; the correlation between the circulating current and the capacitor voltage was illustrated. Reference [25] proposed a closed-loop modelling method, in which the calculation accuracy of an MMC model was improved. Although the mathematical model of the MMC has been studied in the above papers, none of these can be applied to MMCs in transformer-less applications. Due to the reduction in the converter transformer, the current flow loop is changed; consequently, there is a zero-sequence current in the ac side of the MMC. As a result, the mathematical expressions and harmonic performances of the electrical quantities are different. Thus, the existing MMC model is no longer suitable. For solving the above-mentioned problem, a study is carried out in this paper, and the contributions of this research are as follows:

- A highly accurate mathematical analysis model is firstly proposed for MMCs in transformer-less applications. Based on this model, all the electrical quantities of the MMC under the transformer-less connection scheme can be easily calculated, and the interactions among the electrical quantities can be fully seen. It is worth noting that the model is established in the time domain; as a result, the amplitude and phase angle of every harmonic component in each quantity can be directly obtained.

- Taking the zero-sequence current flow loop into consideration, the ac-side and dc-side equivalent models of MMCs in transformer-less applications are studied. The equivalent circuit model is established in both a–b–c stationary and d–q rotating coordinate systems, which can be used for analyzing the relationships among the external electrical quantities of the MMC.

- Case studies under various typical situations are carried out. The waveforms of typical electrical quantities are presented, and the calculated values are compared with the actual waveforms. The comparison results prove that the calculation error is small enough to be negligible; hence the proposed mathematical model can provide a powerful tool for the performance analysis and main circuit parameter design of MMCs in transformer-less applications.

The rest of this paper is structured as follows. In Section 2, a typical circuit diagram of the MMC in transformer-less applications is presented, and the required basic formulas are also given in this section. Section 3 establishes the equivalent circuit models in both a–b–c stationary and d–q rotating coordinate systems. A highly accurate mathematical

analysis model of MMCs in transformer-less applications is proposed in Section 4; the coupled relationships among the ac-side system, the MMC, and the dc-side system are also analyzed. In Section 5, the proposed model is verified under various typical situations, and the effects of changing the circuit parameters are analyzed in case studies. Finally, Section 6 concludes this paper.

2. Foundations

In Figure 1, a typical circuit diagram of an MMC in transformer-less applications is presented [26–28]. The main circuit is composed of three phase legs, and each leg is composed of an upper arm and a lower arm. In each arm, there are N half-bridge submodules (SM). It is worth noting that an arm inductor is connected in the series with submodules in each arm, which is denoted by L_m, and the power losses in each arm are represented by the series connection resistor R_m. The dc-side smoothing reactor is denoted by L_{dc}. In transformer-less applications, the MMC is directly connected to the ac power grid; the equivalent inductance of the ac power grid is represented by L_t.
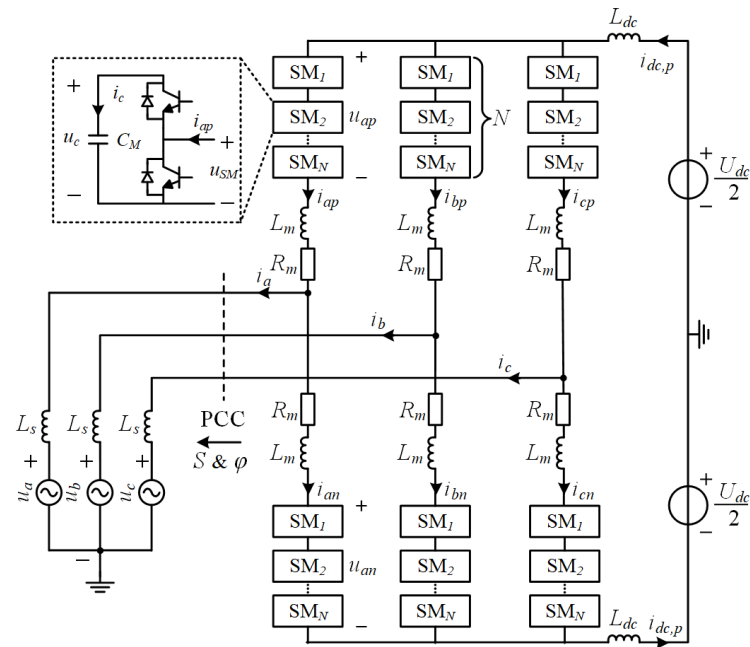

Figure 1. Typical diagram of an MMC in transformer-less applications.

Due to the symmetry of the three phases, phase A is taken as an example for our analysis. The ac-side voltage can be expressed as shown in (1).

$$u_a(t) = U_s \cos(\omega t) \tag{1}$$

where U_s denotes the amplitude of the ac-side power grid voltage.

The ac-side current is denoted by $i_a(t)$, and it can be expressed as shown in (2). It should be noted that, in transformer-less applications, there will be a third-order harmonic component in the ac-side current. This third-order harmonic current will flow from the ac-side power grid across the MMC to the dc-side system.

$$i_a(t) = i_{a,1\omega}(t) + i_{a,3\omega}(t) \tag{2}$$

where

$$\begin{cases} i_{a,1\omega}(t) = I_{m1} \cos(\omega t + \beta_1) \\ i_{a,3\omega}(t) = I_{m3} \cos(3\omega t + \beta_3) \end{cases} \tag{3}$$

In (3), I_{m1} and β_1 denote the amplitude and phase angle of the fundamental current, respectively; I_{m3} and β_3 denote the amplitude and phase angle of the third-order harmonic current, respectively.

Due to the existence of the above-mentioned $i_{a,3rd}(t)$, the dc-side current will contain not only the dc component but also the third-order harmonic component. The dc-side currents in the upper and lower dc buses are denoted by $i_{dc,p}(t)$ and $i_{dc,n}(t)$, respectively; and their expressions can be derived as shown in (4).

$$\begin{cases} i_{dc,p}(t) = I_{dc} + \frac{3}{2}i_{a,3rd}(t) \\ i_{dc,n}(t) = I_{dc} - \frac{3}{2}i_{a,3rd}(t) \end{cases} \tag{4}$$

where I_{dc} is the dc component in the dc-side current.

Then, according to Kirchhoff's current law and Figure 1, the upper- and lower-arm currents can be presented as shown in (5) [29,30].

$$\begin{cases} i_{ap}(t) = \frac{I_{dc}}{3} + \frac{i_a(t)}{2} \\ i_{an}(t) = \frac{I_{dc}}{3} - \frac{i_a(t)}{2} \end{cases} \tag{5}$$

where $i_{ap}(t)$ and $i_{an}(t)$ represent the upper- and lower-arm currents, respectively.

3. Equivalent Circuit Model for MMCs in Transformer-Less Applications

Based on Kirchhoff's voltage law and the circuit diagram shown in Figure 1, the following equations can be obtained:

$$L_s \frac{di_a(t)}{dt} + u_a == -R_m i_{ap} - L_m \frac{di_{ap}(t)}{dt} - u_{ap} - L_{dc} \frac{di_{dc,p}(t)}{dt} + \frac{U_{dc}}{2} \tag{6}$$

$$L_s \frac{di_a(t)}{dt} + u_a == R_m i_{an} + L_m \frac{di_{an}(t)}{dt} + u_{an} + L_{dc} \frac{di_{dc,n}(t)}{dt} - \frac{U_{dc}}{2} \tag{7}$$

where $u_{ap}(t)$ and $u_{an}(t)$ are the upper- and lower-arm voltages, respectively; U_{dc} denotes the dc-side voltage.

Equations (6) and (7) present the relationships among the arm voltage, arm current, dc-side voltage, ac-side current, and ac-side voltage in MMCs. We can define the differential voltage $u_{diff,a}(t)$ and the common-mode voltage $u_{com,a}(t)$ as shown in (8).

$$\begin{cases} u_{diff,a}(t) = \frac{u_{an}(t) - u_{ap}(t)}{2} \\ u_{com,a}(t) = \frac{u_{an}(t) + u_{ap}(t)}{2} \end{cases} \tag{8}$$

Based on (6)–(8), the differential voltage and common-mode voltage can be derived as follows:

$$u_{diff,a}(t) = u_{diff,1\omega}(t) + u_{diff,3\omega}(t) \tag{9}$$

$$u_{com,a}(t) = \frac{U_{dc}}{2} - \frac{R_m I_{dc}}{3} \tag{10}$$

where $u_{diff,1\omega}(t)$ and $u_{diff,3\omega}(t)$ denote the fundamental and third-order harmonic components in the differential voltage, respectively, and their expressions are presented in (11).

$$\begin{cases} u_{diff,1\omega}(t) = U_s \cos(\omega t) + \frac{R_m I_{m1}}{2} \cos(\omega t + \beta_1) - \left[L_s + \frac{L_m}{2}\right] \cdot \omega I_{m1} \sin(\omega t + \beta_1) \\ u_{diff,3\omega}(t) = \frac{R_m I_{m3}}{2} \cos(3\omega t + \beta_3) - \left[L_s + \frac{L_m}{2} + \frac{3L_{dc}}{2}\right] \cdot 3\omega I_{m3} \sin(3\omega t + \beta_3) \end{cases} \tag{11}$$

Then, the equivalent circuit model of the MMC used in transformer-less applications can be established based on (9)–(11), which is presented in Figure 2.
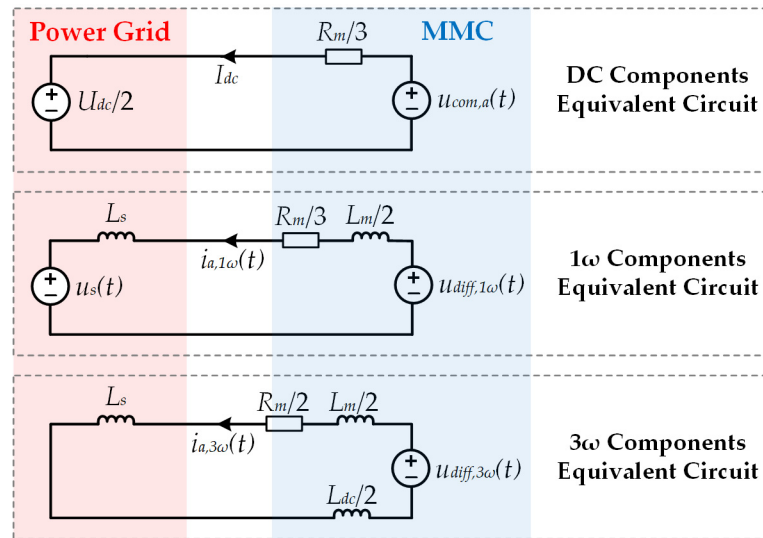
Figure 2. Equivalent circuit model of MMC in transformer-less applications in the three-phase *a–b–c* stationary coordinate system.

In (9)–(11), the equivalent circuit equations are established in the three-phase *a–b–c* stationary coordinate system. Based on the Park transformation [23], it can be transformed into the *d–q* rotating coordinate system. The derived equations are presented in (12).

$$
\begin{cases}
U_{com,dc} = \dfrac{U_{dc}}{2} - \dfrac{R_m I_{dc}}{3} \\
U_{diff,1\omega D} = U_s - \left[L_s + \dfrac{L_m}{2}\right] \cdot \omega I_{m1} \sin(\beta_1) + \dfrac{R_m I_{m1}}{2}\cos(\beta_1) \\
U_{diff,1\omega Q} = -\left[L_s + \dfrac{L_m}{2}\right] \cdot \omega I_{m1}\cos(\beta_1) - \dfrac{R_m I_{m1}}{2}\sin(\beta_1) \\
U_{com,2\omega D} = 0 \\
U_{com,2\omega Q} = 0 \\
U_{diff,3\omega D} = -\left[L_s + \dfrac{L_m}{2} - \dfrac{3L_{dc}}{2}\right] \cdot 3\omega I_{m3}\sin(\beta_3) + \dfrac{R_m I_{m3}}{2}\cos(\beta_3) \\
U_{diff,3\omega Q} = -\left[L_s + \dfrac{L_m}{2} + \dfrac{3L_{dc}}{2}\right] \cdot 3\omega I_{m3}\cos(\beta_3) - \dfrac{R_m I_{m3}}{2}\sin(\beta_3)
\end{cases}
\tag{12}
$$

where $U_{com,dc}$, $U_{com,2\omega D}$, and $U_{com,2\omega Q}$ denote the dc and 2ω components of the common-mode voltage in the *d–q* rotating coordinate system; and $U_{diff,1\omega D}$, $U_{diff,1\omega Q}$, $U_{diff,3\omega D}$, and $U_{diff,3\omega Q}$ are the 1ω and 3ω components of the differential voltage in the *d–q* rotating coordinate system.

It should be noted that, although the equivalent circuit model has been derived in (9)–(12) and Figure 2, the values of the internal electrical quantities in MMCs cannot be known from it. This is because the equivalent circuit model can only describe the external relationships among electrical quantities. Therefore, a highly accurate mathematical analysis model is proposed in the next section for calculating the values of the internal electrical quantities in MMCs in transformer-less applications.

4. Mathematical Analysis Model for MMCs in Transformer-Less Applications

After the establishment of the equivalent circuit model in Section 3, the external relationship of the electrical quantities of the MMC can be known. In this section, a highly accurate mathematical model will be proposed to describe the internal relationship of the electrical quantities of the MMC. In the model, the effects of not using a transformer are fully considered.

The modulation signals in the upper and lower arms, denoted by $M_{ap}(t)$ and $M_{an}(t)$, can be defined as follows:

$$
\begin{cases}
M_{ap}(t) = \dfrac{1}{2} - M_{1\omega}(t) - M_{2\omega}(t) - M_{3\omega}(t) \\
M_{an}(t) = \dfrac{1}{2} + M_{1\omega}(t) - M_{2\omega}(t) + M_{3\omega}(t)
\end{cases}
\tag{13}
$$

where $M_{k\omega}(t)$ denote the k-th order harmonic components, and their expressions are shown in (14).

$$M_{k\omega}(t) = A_k \cos(k\omega t + \alpha_k), k = 1, 2, \text{ and } 3 \tag{14}$$

In (14), A_k and α_k denote the amplitude and phase angle of the k-th order harmonic components in the modulation signals, respectively.

The relationships between the arm currents and the capacitor currents can be expressed as shown in (15), and the relationships between the capacitor currents and the capacitor voltage can be expressed as shown in (18).

$$\begin{cases} i_{cap,ap}(t) = M_{ap}(t) \cdot i_{ap}(t) \\ i_{cap,an}(t) = M_{an}(t) \cdot i_{an}(t) \end{cases} \tag{15}$$

where $i_{cap,ap}(t)$ and $i_{cap,an}(t)$ denote the capacitor currents in the upper and lower arms, respectively.

In the capacitor currents, the dc component should be zero; otherwise, it can lead to a constant increment of SM capacitor voltages, which means that the converter system is not stable. Thus, the following equivalent equation can be derived:

$$\int_t^{t+T} i_{cap,ap}(t)\, dt = 0 \tag{16}$$

Substituting (2)–(5) and (13)–(15) into (16), the expression of the dc-side current can be obtained as follows:

$$I_{dc} = \frac{3A_1 I_{m1}}{2} \cos(\alpha_1 - \beta_1) + \frac{3A_3 I_{m3}}{2} \cos(\alpha_3 - \beta_3) \tag{17}$$

The SM capacitor voltage can be derived by integrating the capacitor current, which is presented in (18).

$$\begin{cases} u_{cap,ap}(t) = U_{c,dc} + \frac{1}{C_M} \int i_{cap,ap}(t)\, dt \\ u_{cap,an}(t) = U_{c,dc} + \frac{1}{C_M} \int i_{cap,an}(t)\, dt \end{cases} \tag{18}$$

where $u_{cap,ap}(t)$ and $u_{cap,an}(t)$ denote the SM capacitor voltages in the upper and lower arms, respectively; and C_M denotes the capacitance of the SM capacitor.

Then, substituting (2)–(5) and (13)–(15) into (18), the expression of the SM capacitor voltage can be derived as follows (19):

$$\begin{cases} u_{cap,ap}(t) = U_{c,dc} + u_{c,1\omega}(t) + u_{c,2\omega}(t) + u_{c,3\omega}(t) \\ u_{cap,an}(t) = U_{c,dc} - u_{c,1\omega}(t) + u_{c,2\omega}(t) - u_{c,3\omega}(t) \end{cases}, k = 1, 2, \text{ and } 3 \tag{19}$$

where $u_{c,k\omega}(t)$ is the k-th order harmonic components in the SM capacitor voltages.

$$\begin{cases} u_{c,1\omega}(t) = -\frac{A_1 I_{dc}}{3\omega C_M} \sin(\omega t + \alpha_1) + \frac{I_{m1}}{4\omega C_M} \sin(\omega t + \beta_1) - \frac{A_2 I_{m3}}{4\omega C_M} \sin(\omega t - \alpha_2 + \beta_3) \\ \qquad - \frac{A_2 I_{m1}}{4\omega C_M} \sin(\omega t + \alpha_2 - \beta_1) \\ u_{c,2\omega}(t) = -\frac{A_2 I_{dc}}{6\omega C_M} \sin(2\omega t + \alpha_2) - \frac{A_3 I_{m1}}{8\omega C_M} \sin(2\omega t + \alpha_3 - \beta_1) - \frac{A_1 I_{m1}}{8\omega C_M} \sin(2\omega t + \alpha_1 + \beta_1) \\ \qquad - \frac{A_1 I_{m3}}{8\omega C_M} \sin(2\omega t - \alpha_1 + \beta_3) \\ u_{c,3\omega}(t) = \frac{I_{m3}}{12\omega C_M} \sin(3\omega t + \beta_3) - \frac{A_3 I_{dc}}{9\omega C_M} \sin(3\omega t + \alpha_3) - \frac{A_2 I_{m1}}{12\omega C_M} \sin(3\omega t + \alpha_2 + \beta_1) \\ u_{c,4\omega}(t) = -\frac{A_3 I_{m1}}{16\omega C_M} \sin(4\omega t + \alpha_3 + \beta_1) - \frac{A_1 I_{m3}}{16\omega C_M} \sin(4\omega t + \alpha_1 + \beta_3) \\ u_{c,5\omega}(t) = -\frac{A_2 I_{m3}}{20\omega C_M} \sin(5\omega t + \alpha_2 + \beta_3) \\ u_{c,6\omega}(t) = -\frac{A_3 I_{m3}}{24\omega C_M} \sin(6\omega t + \alpha_3 + \beta_3) \end{cases} \tag{20}$$

In (12), the expressions of differential and common-mode voltages are established by the external electrical quantities. Based on the equations derived in Section 4, the expressions of differential and common-mode voltages can also be established by the internal electrical quantities of the MMC.

Equation (21) shows the relationships between the arm voltage and the SM capacitor voltage.

$$\begin{cases} u_{ap}(t) = N \cdot M_{ap}(t) \cdot u_{cap,ap}(t) \\ u_{an}(t) = N \cdot M_{an}(t) \cdot u_{cap,an}(t) \end{cases} \tag{21}$$

Substituting (21) into (8), the differential and common-mode voltages can be expressed as shown in (22).

$$\begin{cases} u_{diff,a}(t) = N \cdot \frac{M_{an}(t) \cdot u_{cap,an}(t) - M_{ap}(t) \cdot u_{cap,ap}(t)}{2} \\ u_{com,a}(t) = N \cdot \frac{M_{an}(t) \cdot u_{cap,an}(t) + M_{ap}(t) \cdot u_{cap,ap}(t)}{2} \end{cases} \tag{22}$$

Then, based on (13), (19) and (22), the mathematical expressions of the differential and common-mode voltages can be established in the d–q rotating coordinate system by using the internal electrical quantities of the MMC; the obtained equations are presented in (23).

$$
\begin{cases}
V_{com,dc} = \frac{NU_{c,0}}{2} - \frac{A_1 A_2 I_{m1} N}{16\omega C_M}\sin(\alpha_1 - \alpha_2 + \beta_1) - \frac{A_2 A_3 I_{m1} N}{48\omega C_M}\sin(\alpha_2 - \alpha_3 + \beta_1) \\
\qquad + \frac{A_1 I_{m1} N}{8\omega C_M}\sin(\alpha_1 - \beta_1) - \frac{3A_1 A_2 I_{m3} N}{16\omega C_M}\sin(\alpha_1 + \alpha_2 - \beta_3) + \frac{A_3 I_{m3} N}{24\omega C_M}\sin(\alpha_3 - \beta_3) \\
V_{diff,1\omega D} = A_1 NU_{c,0}\cos(\alpha_1) + \frac{A_1 I_{dc} N}{6\omega C_M}\sin(\alpha_1) - \frac{A_1 A_3 I_{m3} N}{32\omega C_M}\sin(\alpha_1 - \alpha_3 + \beta_3) \\
\qquad - \frac{A_1 A_2 I_{dc} N}{12\omega C_M}\sin(\alpha_1 - \alpha_2) + \frac{A_1^2 I_{m3} N}{16\omega C_M}\sin(2\alpha_1 - \beta_3) + \frac{A_1 A_3 I_{m3} N}{16\omega C_M}\sin(\alpha_1 + \alpha_3 - \beta_3) \\
\qquad - \frac{A_2 I_{m3} N}{6\omega C_M}\sin(\alpha_2 - \beta_3) + \frac{A_2^2 I_{m3} N}{8\omega C_M}\sin(2\alpha_2 - \beta_3) - \frac{A_2 A_3 I_{dc} N}{36\omega C_M}\sin(\alpha_2 - \alpha_3) \\
\qquad - \left(\frac{1}{8\omega C_M} + \frac{A_1^2}{16\omega C_M} - \frac{A_2^2}{12\omega C_M} - \frac{A_3^2}{32\omega C_M}\right)I_{m1} N\sin(\beta_1) \\
V_{diff,1\omega Q} = -A_1 NU_{c,0}\sin(\alpha_1) + \frac{A_1 I_{dc} N}{6\omega C_M}\cos(\alpha_1) - \frac{A_1 A_3 I_{m3} N}{32\omega C_M}\cos(\alpha_1 - \alpha_3 + \beta_3) \\
\qquad + \frac{A_1 A_2 I_{dc} N}{12\omega C_M}\cos(\alpha_1 - \alpha_2) - \frac{A_1^2 I_{m3} N}{16\omega C_M}\cos(2\alpha_1 - \beta_3) + \frac{A_1 A_3 I_{m3} N}{16\omega C_M}\cos(\alpha_1 + \alpha_3 - \beta_3) \\
\qquad + \frac{A_2 I_{m3} N}{6\omega C_M}\cos(\alpha_2 - \beta_3) + \frac{A_2^2 I_{m3} N}{8\omega C_M}\cos(2\alpha_2 - \beta_3) + \frac{A_2 A_3 I_{dc} N}{36\omega C_M}\cos(\alpha_2 - \alpha_3) \\
\qquad - \left(\frac{1}{8\omega C_M} + \frac{A_1^2}{16\omega C_M} - \frac{A_2^2}{12\omega C_M} - \frac{A_3^2}{32\omega C_M}\right)I_{m1} N\cos(\beta_1) \\
V_{com,2\omega D} = -A_2 NU_{c,0}\cos(\alpha_2) + \frac{A_1^2 I_{dc} N}{6\omega C_M}\sin(2\alpha_1) - \frac{A_2 I_{dc} N}{12\omega C_M}\sin(\alpha_2) - \frac{A_2 A_3 I_{m3} N}{8\omega C_M}\sin(\alpha_2 + \alpha_3 - \beta_3) \\
\qquad + \frac{A_1 A_2 I_{m1} N}{8\omega C_M}\sin(\alpha_1 + \alpha_2 - \beta_1) + \frac{A_3 I_{m1} N}{16\omega C_M}\sin(\alpha_3 - \beta_1) - \frac{3A_1 I_{m1} N}{16\omega C_M}\sin(\alpha_1 + \beta_1) \\
\qquad + \frac{A_1 A_3 I_{dc} N}{9\omega C_M}\sin(\alpha_1 - \alpha_3) - \frac{A_1 A_2 I_{m1} N}{24\omega C_M}\sin(\alpha_1 - \alpha_2 - \beta_1) + \frac{5A_1 A_2 I_{m3} N}{32\omega C_M}\sin(\alpha_1 - \alpha_2 + \beta_3) \\
\qquad + \frac{5A_1 I_{m3} N}{48\omega C_M}\sin(\alpha_1 - \beta_3) + \frac{3A_2 A_3 I_{m1} N}{32\omega C_M}\sin(\alpha_2 - \alpha_3 - \beta_1) + \frac{A_2 A_3 I_{m3} N}{40\omega C_M}\sin(\alpha_2 - \alpha_3 + \beta_3) \\
V_{com,2\omega Q} = +A_2 NU_{c,0}\sin(\alpha_2) + \frac{A_1^2 I_{dc} N}{6\omega C_M}\cos(2\alpha_1) - \frac{A_2 I_{dc} N}{12\omega C_M}\cos(\alpha_2) - \frac{A_2 A_3 I_{m3} N}{8\omega C_M}\cos(\alpha_2 + \alpha_3 - \beta_3) \\
\qquad + \frac{A_1 A_2 I_{m1} N}{8\omega C_M}\cos(\alpha_1 + \alpha_2 - \beta_1) + \frac{A_3 I_{m1} N}{16\omega C_M}\cos(\alpha_3 - \beta_1) - \frac{3A_1 I_{m1} N}{16\omega C_M}\cos(\alpha_1 + \beta_1) \\
\qquad - \frac{A_1 A_3 I_{dc} N}{9\omega C_M}\cos(\alpha_1 - \alpha_3) + \frac{A_1 A_2 I_{m1} N}{24\omega C_M}\cos(\alpha_1 - \alpha_2 - \beta_1) + \frac{5A_1 A_2 I_{m3} N}{32\omega C_M}\cos(\alpha_1 - \alpha_2 + \beta_3) \\
\qquad - \frac{5A_1 I_{m3} N}{48\omega C_M}\cos(\alpha_1 - \beta_3) - \frac{3A_2 A_3 I_{m1} N}{32\omega C_M}\cos(\alpha_2 - \alpha_3 - \beta_1) + \frac{A_2 A_3 I_{m3} N}{40\omega C_M}\cos(\alpha_2 - \alpha_3 + \beta_3) \\
V_{diff,3\omega D} = A_3 NU_{c,0}\cos(\alpha_3) + \frac{A_3 I_{dc} N}{18\omega C_M}\sin(\alpha_3) + \frac{A_2 I_{m1} N}{6\omega C_M}\sin(\alpha_2 + \beta_1) - \frac{A_1 A_2 I_{dc} N}{4\omega C_M}\sin(\alpha_1 + \alpha_2) \\
\qquad - \frac{A_2^2 I_{m1} N}{8\omega C_M}\sin(2\alpha_2 - \beta_1) - \frac{A_1^2 I_{m1} N}{16\omega C_M}\sin(2\alpha_1 + \beta_1) - \frac{A_1 A_3 I_{m1} N}{16\omega C_M}\sin(\alpha_1 + \alpha_3 - \beta_1) \\
\qquad + \frac{A_1 A_3 I_{m1} N}{32\omega C_M}\sin(\alpha_1 - \alpha_3 - \beta_1) - \left(\frac{1}{24\omega C_M} + \frac{3A_1^2}{32\omega C_M} + \frac{3A_2^2}{20\omega C_M} + \frac{A_3^2}{48\omega C_M}\right)I_{m3} N\sin(\beta_3) \\
V_{diff,3\omega Q} = -A_3 NU_{c,0}\sin(\alpha_3) + \frac{A_3 I_{dc} N}{18\omega C_M}\cos(\alpha_3) + \frac{A_2 I_{m1} N}{6\omega C_M}\cos(\alpha_2 + \beta_1) - \frac{A_1 A_2 I_{dc} N}{4\omega C_M}\cos(\alpha_1 + \alpha_2) \\
\qquad - \frac{A_2^2 I_{m1} N}{8\omega C_M}\cos(2\alpha_2 - \beta_1) - \frac{A_1^2 I_{m1} N}{16\omega C_M}\cos(2\alpha_1 + \beta_1) - \frac{A_1 A_3 I_{m1} N}{16\omega C_M}\cos(\alpha_1 + \alpha_3 - \beta_1) \\
\qquad - \frac{A_1 A_3 I_{m1} N}{32\omega C_M}\cos(\alpha_1 - \alpha_3 - \beta_1) - \left(\frac{1}{24\omega C_M} + \frac{3A_1^2}{32\omega C_M} + \frac{3A_2^2}{20\omega C_M} + \frac{A_3^2}{48\omega C_M}\right)I_{m3} N\cos(\beta_3)
\end{cases} \tag{23}
$$

where the expressions of $V_{com,dc}$, $V_{diff,1\omega D}$, $V_{diff,1\omega Q}$, $V_{com,2\omega D}$, $V_{com,2\omega Q}$, $V_{diff,3\omega D}$ and $V_{diff,3\omega Q}$ are established by the internal electrical quantities of the MMC; $V_{com,dc}$, $V_{com,2\omega D}$ and $V_{com,2\omega Q}$ denote the dc and 2ω components of the common-mode voltage in the d–q rotating coordinate system, respectively; and $V_{diff,1\omega D}$, $V_{diff,1\omega Q}$, $V_{diff,3\omega D}$ and $V_{diff,3\omega Q}$ are the 1ω and 3ω components of the differential voltage in the d–q rotating coordinate system, respectively.

In (12) and (23), the differential and common-mode voltages are derived by two different approaches; hence, the equivalent equations in (24) can be established.

$$\begin{cases} U_{com,dc} = V_{com,dc} \\ U_{diff,1\omega D} = V_{diff,1\omega D} \\ U_{diff,1\omega Q} = V_{diff,1\omega Q} \\ U_{com,2\omega D} = 0 \\ U_{com,2\omega Q} = 0 \\ U_{diff,3\omega D} = V_{diff,3\omega D} \\ U_{diff,3\omega D} = V_{diff,3\omega D} \end{cases} \tag{24}$$

The detailed expressions of $U_{com,dc}$, $U_{diff,1\omega D}$, $U_{diff,1\omega Q}$, $U_{com,2\omega D}$, $U_{com,2\omega Q}$, $U_{diff,3\omega D}$, $U_{diff,3\omega Q}$, $V_{com,dc}$, $V_{diff,1\omega D}$, $V_{diff,1\omega Q}$, $V_{com,2\omega D}$, $V_{com,2\omega Q}$, $V_{diff,3\omega D}$ and $V_{diff,3\omega Q}$ are presented in (12) and (23).

Then, based on the above-derived equations, the electrical quantities of the MMC in transformer-less applications can be calculated. For convenience, a flow chart showing the detailed calculation procedure is presented in Figure 3, and the calculation procedure is explained as follows:
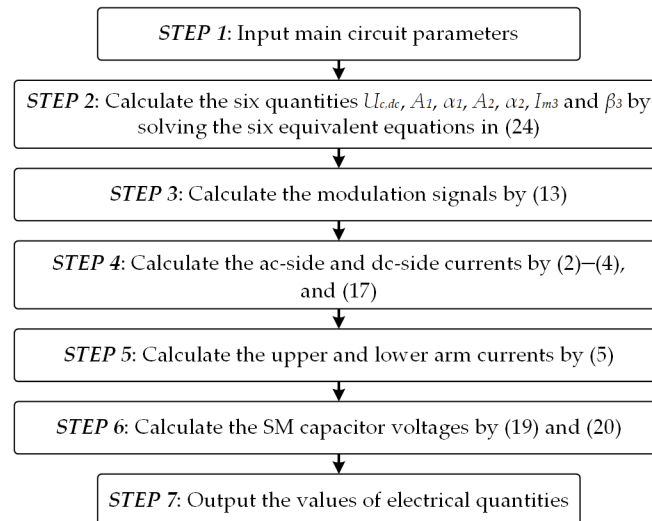

Figure 3. Flow chart for calculating the time-varying values of electrical quantities based on the proposed mathematical model.

- *STEP 1*: The main circuit parameters of the MMC are input. These parameters include the SM capacitance C_M, number of SM in one arm N, arm inductance L_m, dc-side rated voltage U_{dc}, ac-side rated voltage U_s, inductance of dc-current reactor L_{dc}, and equivalent ac system inductance L_s. These are the prerequisite parameters determining an MMC system.
- *STEP 2*: The six unknowns ($U_{c,dc}$, A_1, α_1, A_2, α_2, I_{m3}, and β_3) can be solved from the derived six equivalent equations shown in (24). The equivalent equations can be easily solved by numerical methods, such as Newton's method, which is well known [31].
- *STEP 3*: After the amplitude and phase angle of the modulation signal are obtained, its time-varying values can be calculated by equations shown in (13).
- *STEP 4*: The ac-side and dc-side currents can be calculated by the equations derived in Sections 3 and 4. The equations of the ac-side current are shown in (2) and (3); the equations of the dc-side current are shown in (4) and (17).
- *STEP 5*: The upper- and lower-arm currents can be directly calculated by (5).
- *STEP 6*: The SM capacitor voltages in the upper and lower arms can be directly calculated based on the derived equations shown in (19) and (20).
- *STEP 7*: Finally, the time-varying values of the electrical quantities in the MMC can be obtained.

5. Case Study and Verification

To verify the accuracy of the proposed mathematical model, cases under different typical operation situations are studied in this section by using the RT-Lab platform [32–34]. The topology of the MMC used is presented in Figure 1. The main circuit parameters are shown in Table 1.

Table 1. Main circuit parameters of the MMC used.

Parameter	Values
Rated power	100 MVA
Rated system frequency	50 Hz
Rated line voltage	110 kV
Dc link voltage	±100 kV
Number of SMs per arm	100
SM capacitor capacitance	3000 μF
Arm inductance	10 mH
Equivalent ac system inductance	10 mH
Dc current reactor	10 mH

5.1. Converter System Current in Transformer-Less Applications

The system currents in transformer-less applications are presented in Figure 4. The power condition is "$S = 100$ MW, $\varphi = 0$ rad". The actual waveforms are denoted by the colored curves, and the calculated values are denoted by the dots and dashed lines. From the top to the bottom, the four sub-figures show the comparison results of the output current of phase a, the upper- and lower-arm currents, the ac-side zero-sequence current, and the positive and negative dc bus currents. The calculated values are obtained based on the proposed mathematical model in this paper.
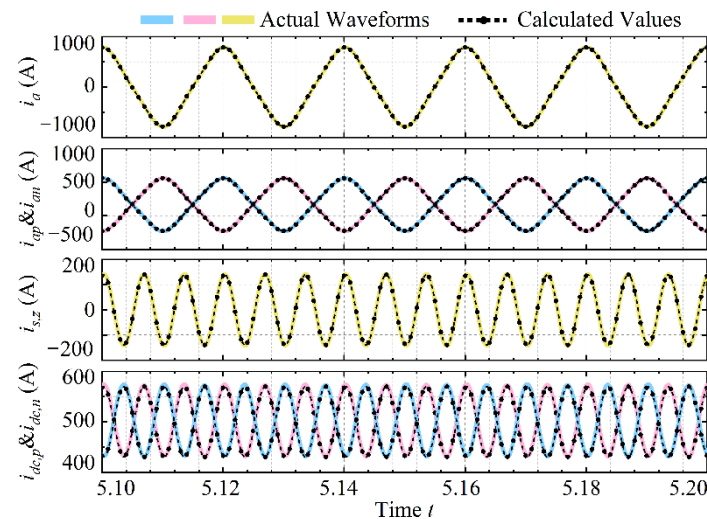

Figure 4. Comparisons between the calculated values and the actual waveforms under the power condition of "$S = 100$ MW, $\varphi = 0$ rad". The waveforms include the system current $i_a(t)$, the upper and lower arm currents $i_{ap}(t)$ and $i_{an}(t)$, the ac-side zero-sequence current $i_{s,z}(t)$, and the dc bus currents $i_{dc,p}(t)$ and $i_{dc,n}(t)$.

As seen from Figure 5, the calculated values fit well with the actual waveforms, which proves that the established mathematical model is accurate. It can be seen that the amplitude of the ac-side zero-sequence current is 140.1 A, and the frequency of the current is 150 Hz; moreover, the dc bus currents contain not only the dc component but also the ac component, which is at a frequency of 150 Hz. This can confirm that there is a third-order harmonic current flowing among the ac, MMC, and dc systems when the connected transformer is not used. This third-order harmonic current can be accurately seen in the proposed mathematical model.
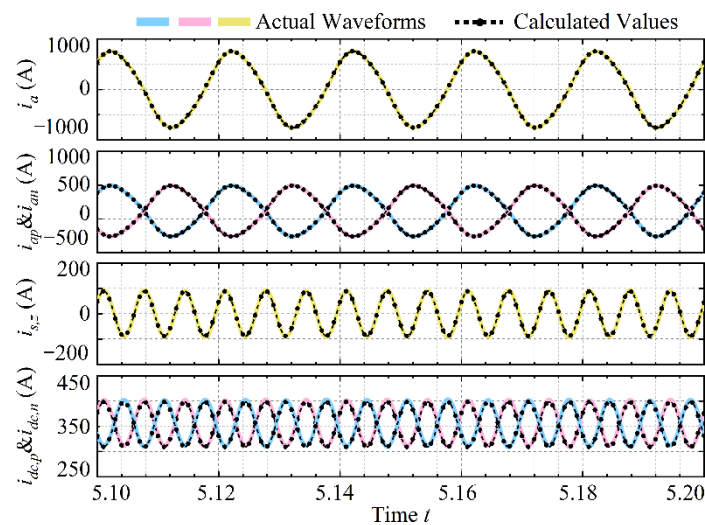
Figure 5. Comparisons between the calculated values and the actual waveforms under the power condition of "S = 100 MW, $\varphi = \pi/4$ rad". The waveforms include the system current $i_a(t)$, the upper and lower arm currents $i_{ap}(t)$ and $i_{an}(t)$, the ac-side zero-sequence current $i_{s,z}(t)$, and the dc bus currents $i_{dc,p}(t)$ and $i_{dc,n}(t)$.

For further verifications, the power condition is changed to "S = 100 MW, $\varphi = \pi/4$ rad", and the waveforms are shown in Figure 5. Similarly, the actual waveforms are denoted by the colored curves, and the calculated values are denoted by the dots and dashed lines.

As seen from Figure 5, although the power condition is changed, the calculated values are still consistent with the actual waveforms. This can further prove that the proposed mathematical model is accurate. Moreover, the third-order harmonic current that flows among the ac, MMC and dc systems is highly related with the power condition of the MMC. The amplitude of the ac-side zero-sequence current is changed to 89.5 A when the power factor angle changes to $\varphi = \pi/4$ rad. This change can be fully seen in the established mathematical model in this paper.

5.2. SM Capacitor Voltage and Modulation Signals

Based on the proposed mathematical model, the values of the SM capacitor voltages and modulation signals can be easily calculated. To verify the calculation accuracy, the comparisons are presented. Figures 6a and 6b shows the waveforms under the power conditions of "S = 100 MW, φ = 0 rad" and "S = 100 MW, $\varphi = \pi/4$ rad", respectively. As seen from the comparison results, the curves of calculated values always coincide with the actual waveforms under different power conditions, and the calculation errors are small enough to be negligible.
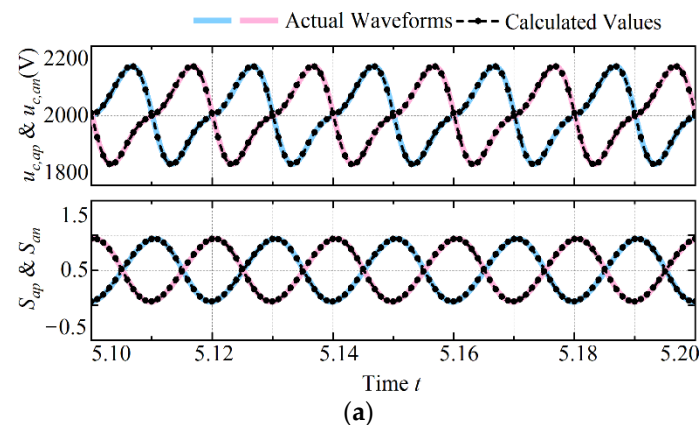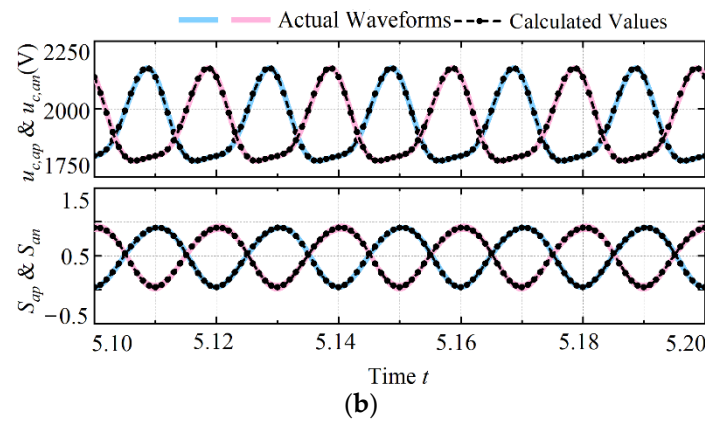

(a)

Figure 6. *Cont.*

Figure 6. The verification of calculation accuracy of the SM capacitor voltage and modulation signal in the proposed model by comparisons between the calculated values and the actual waveforms under different power conditions: (**a**) under the power condition of "S = 100 MW, φ = 0 rad"; (**b**) under the power condition of "S = 100 MW, φ = $\pi/4$ rad".

5.3. Influence of Main Circuit Parameters

Furthermore, to verify the accuracy of the proposed model under different main circuit parameters, three typical situations are selected for case studies, which are stated as follows.

- *Situation 1:* The arm inductance L_m is changed to be 20 mH. The waveforms of electrical quantities are presented in Figure 7.
- *Situation 2:* The equivalent inductance of the ac-side system L_s is changed to be 20 mH. The waveforms of electrical quantities are presented in Figure 8.
- *Situation 3:* The inductance of the dc-side current reactor L_{dc} is changed to be 20 mH. The waveforms of electrical quantities are presented in Figure 9.

In Figures 7–9, sub-figure (a) shows the waveforms of the dc-side current, SM capacitor voltages, and modulation signals; sub-figure (b) shows the waveforms of the ac-side current, arm currents, and ac-side zero-sequence current. The actual waveforms are denoted by the colored curves, and the calculated values are denoted by the dots and dashed lines.

Figure 7 presents the waveform and calculated values when the arm inductance L_m is changed to be 20 mH. It can be seen that the calculated values still fit well with the actual waveforms. This can prove that the accuracy of the proposed method is not affected by the circuit parameter modification, the established mathematical model is still highly accurate when the arm inductance is changed.

In Figure 8, the equivalent inductance of the ac-side system L_s is changed to be 20 mH. Comparing Figure 8 with Figure 7, the waveforms are influenced by the parameter modification. Nevertheless, the calculated values are still consistent with the actual waveforms; hence, the influence of parameter modification can be seen in the proposed mathematical model.

Figure 9 presents a situation in which the inductance of the dc-side current reactor L_{dc} is changed to be 20 mH. The established model is still highly accurate in this situation. Moreover, it is worth noting that the fluctuation value of the ac-side zero-sequence current is significantly influenced by the inductance of the dc-side current reactor L_{dc}. Thus, when the MMC is used in transformer-less applications, the selection of L_{dc} should consider the influence of the ac-side zero-sequence current. Since the influence can be accurately seen in the proposed mathematical model, this paper can provide a useful tool in the main circuit parameter selection of MMCs.

From the comparisons above, it can be confirmed that the accuracy of the proposed method is not affected by the circuit parameter modification, the established mathematical model is always highly accurate regardless of the value of the adopted circuit parameters.
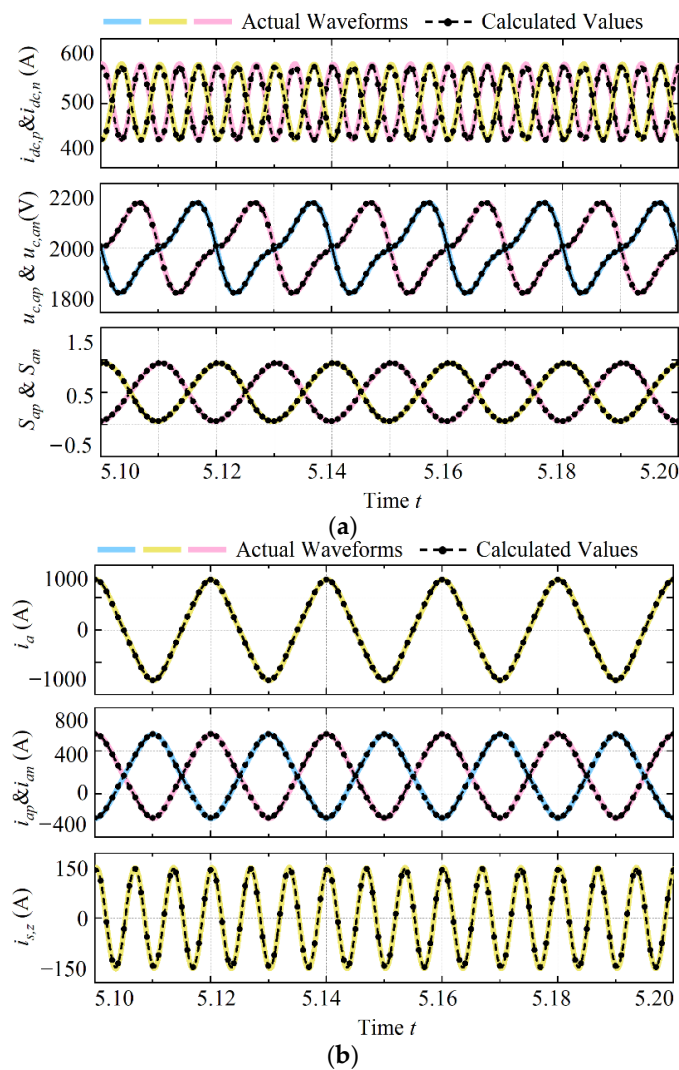
(a)

(b)

Figure 7. Influences on the typical electrical quantities when the arm inductance L_m is changed to be 20 mH; (**a**) waveform of the dc-side current, SM capacitor voltages, and modulation signals; (**b**) waveform of the ac-side current, arm currents, and ac-side zero-sequence current.
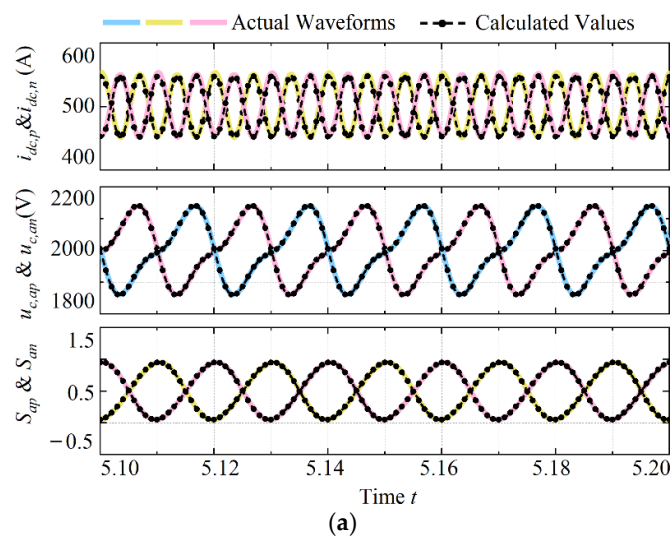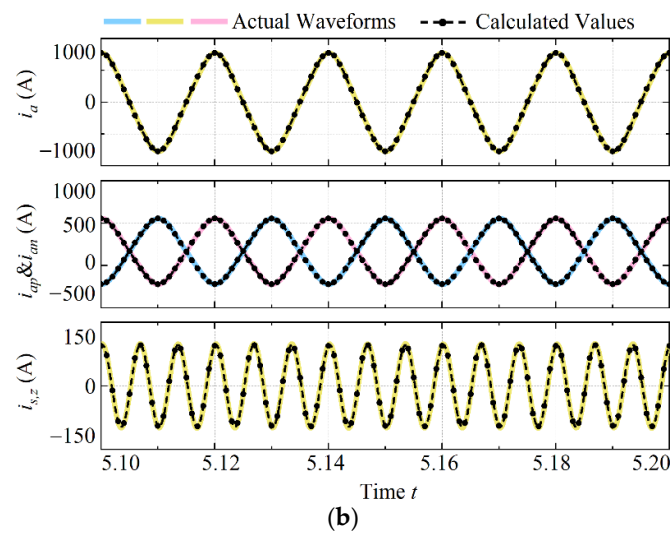

(a)

Figure 8. *Cont.*

Figure 8. Influences on the typical electrical quantities when the equivalent system inductance L_s is set to be 20 mH; (**a**) waveform of the dc-side current, SM capacitor voltages, and modulation signals; (**b**) waveform of the ac-side current, arm currents, and ac-side zero-sequence current.

Figure 9. Influences on the typical electrical quantities when the dc-current reactor L_{dc} is set to be 20 mH; (**a**) waveform of the dc-side current, SM capacitor voltages, and modulation signals; (**b**) waveform of the ac-side current, arm currents, and ac-side zero-sequence current.
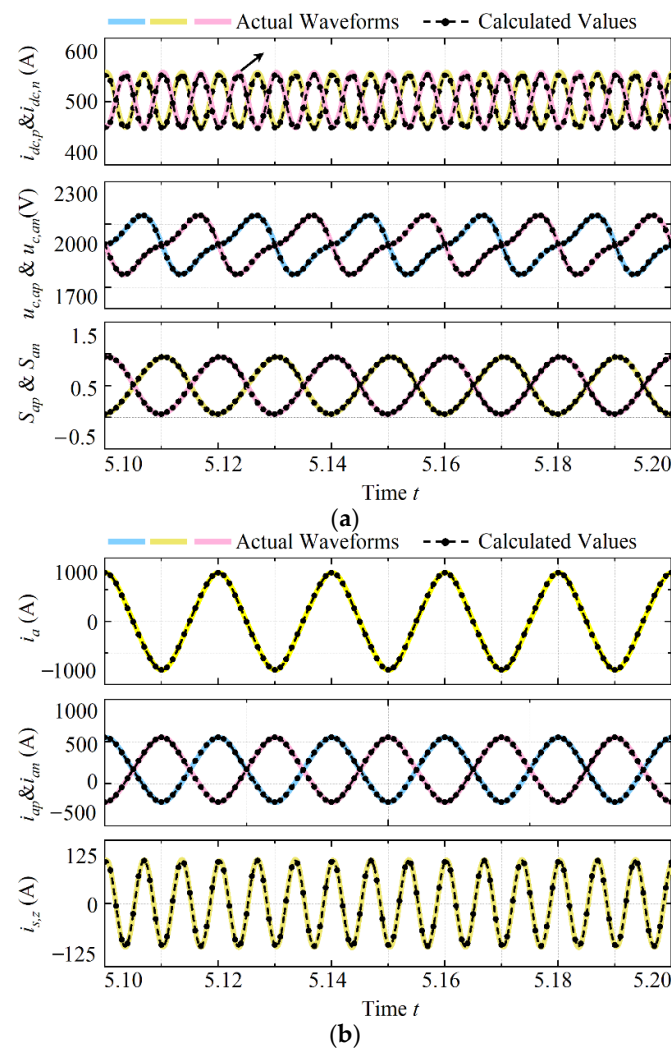
6. Conclusions

A transformer-less connection scheme can provide a more economical solution for MMC-based systems. However, since the reduction in the converter transformer can make the existing MMC model no longer suitable, analyses of MMCs in transformer-less applications are difficult. This can hinder the development and application of the transformer-less connection scheme in MMC-based systems.

In this paper, a highly accurate mathematical analysis model is proposed. Based on this model, all the electrical quantities of the MMC under the transformer-less connection scheme can be easily calculated, and the interactions among the electrical quantities can be fully seen. In addition, the amplitude and phase angle of every harmonic component in each quantity can be directly obtained. In the case study section, the proposed model is verified under various typical situations by comparing the calculated values with the actual waveforms. The comparison results prove that the proposed mathematical model is highly accurate in all situations, and the calculation error is small enough to be negligible.

The mathematical model established in this paper can provide a powerful steady-state analysis tool for MMCs in transformer-less applications. Based on this study, further research can be carried out on the transformer-less connection scheme in MMC-based systems, such as for operation region analyses, circuit parameter selection and steady-state performance optimization. Due to the economy of the transformer-less connection scheme, this study is significant not only for DC power supply technology but also modern power systems.

References

1. Rocabert, J.; Luna, A.; Blaabjerg, F.; Rodríguez, P. Control of power converters in AC microgrids. *IEEE Trans. Power Electron.* **2012**, *27*, 4734–4749. [CrossRef]
2. Debnath, S.; Qin, J.; Bahrani, B.; Saeedifard, M.; Barbosa, P. Operation, control, and applications of the modular multilevel converter: A review. *IEEE Trans. Power Electron.* **2015**, *30*, 37–53. [CrossRef]
3. Liu, Z.; Li, K.-J.; Guo, Z.; Wang, J.; Qian, J. Evaluating the over-modulation risk of modular multilevel converters by using dynamic modulation ratio. *IEEE J. Emerg. Sel. Top. Power Electron.* **2021**. [CrossRef]
4. Ansari, J.A.; Liu, C.; Khan, S.A. MMC based MTDC grids: A detailed review on issues and challenges for operation, control and protection schemes. *IEEE Access* **2020**, *8*, 168154–168165. [CrossRef]
5. Yu, X.; Zhao, B.; Wang, S.; Wang, T.; Zhang, L. A topology analysis-based MMC-HVDC grid transmission capacity calculation method. *Symmetry* **2021**, *13*, 822. [CrossRef]
6. Liu, Z.; Li, K.; Wang, J.; Li, L. A side-effect-free method of reducing capacitance requirement for modular multilevel converters. *High Volt.* **2022**, *7*, 461–472. [CrossRef]
7. Farias, J.A.V.M.; Cupertino, A.F.; Pereira, H.A.; Seleme, S.I.; Teodorescu, R. On converter fault tolerance in MMC-HVDC systems: A comprehensive survey. *IEEE J. Emerg. Sel. Top. Power Electron.* **2021**, *9*, 7459–7470. [CrossRef]
8. Wang, S.; Qin, S.; Yang, P.; Sun, Y.; Zhao, B.; Yin, R.; Sun, S.; Tian, C.; Zhao, Y. Research on the new topology and coordinated control strategy of renewable power generation connected MMC-Based DC power grid integration system. *Symmetry* **2021**, *13*, 1965. [CrossRef]
9. Liu, Z.; Li, K.; Sun, Y.; Wang, J.; Wang, Z.; Sun, K.; Wang, M. A steady-state analysis method for modular multilevel converters connected to permanent magnet synchronous generator-based wind energy conversion systems. *Energies* **2018**, *11*, 461. [CrossRef]
10. Novakovic, B.; Nasiri, A. Modular multilevel converter for wind energy storage applications. *IEEE Trans. Ind. Electron.* **2017**, *64*, 8867–8876. [CrossRef]
11. Zhou, Y.; Jiang, D.; Hu, P.; Guo, J.; Liang, Y.; Lin, Z. A prototype of modular multilevel converters. *IEEE Trans. Power Electron.* **2014**, *29*, 3267–3278. [CrossRef]
12. Nguyen, T.H.; Hosani, K.A.; Moursi, M.S.E.; Blaabjerg, F. An overview of modular multilevel converters in HVDC transmission systems with STATCOM operation during pole-to-pole DC short circuits. *IEEE Trans. Power Electron.* **2019**, *34*, 4137–4160. [CrossRef]

13. Ronanki, D.; Williamson, S.S. Modular multilevel converters for transportation electrification: Challenges and opportunities. *IEEE Trans. Transp. Electrif.* **2018**, *4*, 399–407. [CrossRef]

14. Ma, F.; Xu, Q.; He, Z.; Tu, C.; Shuai, Z.; Luo, A.; Li, Y. A railway traction power conditioner using modular multilevel converter and its control strategy for high-speed railway system. *IEEE Trans. Transp. Electrif.* **2016**, *2*, 96–109. [CrossRef]

15. Zhang, B.; Nademi, H. Modeling and harmonic stability of MMC-HVDC with passive circulating current filters. *IEEE Access* **2020**, *8*, 129372–129386. [CrossRef]

16. Miet, G.P.A.; Mieee, O.A.-L.; Mieee, G.B.; Smieee, J.M. Transformerless STATCOM based on a five-level modular multilevel converter. In Proceedings of the 2009 13th European Conference on Power Electronics and Applications, Barcelona, Spain, 8–10 September 2009; pp. 1–10.

17. Mohammadi, P.H.; Bina, M.T. A transformerless medium-voltage STATCOM topology based on extended modular multilevel converters. *IEEE Trans. Power Electron.* **2011**, *26*, 1534–1545.

18. Timofejevs, A.; Gamboa, D.; Liserre, M.; Teodorescu, R.; Chaudhary, S.K. Control of transformerless MMC-HVDC during asymmetric grid faults. In Proceedings of the IECON 2013—39th Annual Conference of the IEEE Industrial Electronics Society, Vienna, Austria, 10–13 November 2013; pp. 2016–2021.

19. Hu, J.; Tang, J.; Mei, Y.; Hu, S.; Li, W.; He, X. Common-mode voltage analysis and suppression in five-level modular composited converter. In Proceedings of the 2017 IEEE Energy Conversion Congress and Exposition (ECCE), Cincinnati, OH, USA, 1–5 October 2017; pp. 4873–4878.

20. Yadav, A.; Singh, S.N.; Das, S.P. Analysis of transformerless mmc and suppression of third order harmonic current. In Proceedings of the 2019 National Power Electronics Conference (NPEC), Tiruchirappalli, India, 13–15 December 2019; pp. 1–6.

21. Yu, Y.; Jiang, D.; Liang, Y.; Chen, J. Research on the transformerless connection mode for DC power distribution system. *J. Eng.* **2019**, *2019*, 3378–3382. [CrossRef]

22. Song, Q.; Liu, W.; Li, X.; Rao, H.; Xu, S.; Li, L. A steady-state analysis method for a modular multilevel converter. *IEEE Trans. Power Electron.* **2013**, *28*, 3702–3713. [CrossRef]

23. Ilves, K.; Antonopoulos, A.; Norrga, S.; Nee, H.-P. Steady-state analysis of interaction between harmonic components of arm and line quantities of modular multilevel converters. *IEEE Trans. Power Electron.* **2012**, *27*, 57–68. [CrossRef]

24. Li, X.; Song, Q.; Liu, W.; Xu, S.; Zhu, Z.; Li, X. Performance analysis and optimization of circulating current control for modular multilevel converter. *IEEE Trans. Ind. Electron.* **2016**, *63*, 716–727. [CrossRef]

25. Wang, J.; Liang, J.; Gao, F.; Dong, X.; Wang, C.; Zhao, B. A closed-loop time-domain analysis method for modular multilevel converter. *IEEE Trans. Power Electron.* **2017**, *32*, 7494–7508. [CrossRef]

26. Perez, M.A.; Bernet, S.; Rodriguez, J.; Kouro, S.; Lizana, R. Circuit topologies, modeling, control schemes, and applications of modular multilevel converters. *IEEE Trans. Power Electron.* **2015**, *30*, 4–17. [CrossRef]

27. Priya, M.; Ponnambalam, P.; Muralikumar, K. Modular-multilevel converter topologies and applications—A review. *IET Power Electron.* **2019**, *12*, 170–183. [CrossRef]

28. Liu, Z.; Li, K.-J.; Guo, Z.; Wang, J.; Qian, J. A comprehensive study on the modulation ratio for modular multilevel converters. *IEEE Trans. Ind. Appl.* **2022**, *58*, 3205–3216. [CrossRef]

29. Li, J.; Konstantinou, G.; Wickramasinghe, H.R.; Pou, J. Operation and control methods of modular multilevel converters in unbalanced AC grids: A review. *IEEE J. Emerg. Sel. Top. Power Electron.* **2019**, *7*, 1258–1271. [CrossRef]

30. Liu, Z.; Li, K.-J.; Wang, J.; Javid, Z.; Wang, M.; Sun, K. Research on capacitance selection for modular multi-level converter. *IEEE Trans. Power Electron.* **2019**, *34*, 8417–8434. [CrossRef]

31. Kelley, C.T. *Solving Nonlinear Equations with Newton's Method (Fundamentals of Algorithms)*; SIAM: Philadelphia, PA, USA, 2003.

32. Dennetière, S.; Saad, H.; Clerc, B.; Mahseredjian, J. Setup and performances of the real-time simulation platform connected to the INELFE control system. *Electr. Power Syst. Res.* **2016**, *138*, 180–187. [CrossRef]

33. Li, G.; Zhang, D.; Xin, Y.; Jiang, S.; Wang, W.; Du, J. Design of MMC hardware-in-the-loop platform and controller test scheme. *CPSS Trans. Power Electron. Appl.* **2019**, *4*, 143–151. [CrossRef]

34. Peralta, J.; Saad, H.; Dennetiere, S.; Mahseredjian, J.; Nguefeu, S. Detailed and averaged models for a 401-level MMC–HVDC system. *IEEE Trans. Power Deliv.* **2012**, *27*, 1501–1508. [CrossRef]